# Effects of Duty Cycle, Current Frequency, and Current Density on Corrosion Behavior of the Plasma Electrolytic Oxidation Coatings on 6061 Al Alloy in Artificial Seawater

MOJTABA VAKILI-AZGHANDI and ARASH FATTAH-ALHOSSEINI

In this study, the effects of duty cycle, current frequency, and current density on corrosion behavior of the plasma electrolytic oxidation (PEO) coatings on 6061 Al alloy in artificial seawater (3.5 wt pct NaCl solution) were investigated. To serve this purpose, the electrical parameters of a unipolar pulsed current were applied during the PEO process on 6061 Al alloy in alkaline silicate electrolyte with and without $Al_2O_3$ nanoparticles. The coating morphology and microstructure were characterized by the scanning electron microscopy. The corrosion behavior and electrochemical response of the specimens treated by plasma electrolytic oxidation were analyzed by the electrochemical impedance spectroscopy and the potentiodynamic polarization in artificial seawater. It was found that PEO coatings formed in the presence of $Al_2O_3$ nanoparticle had lower porosity and exhibited better corrosion behavior compared with the coatings formed in the absence of $Al_2O_3$ nanoparticle in the structure. This can be attributed to the nanoparticles' incorporation and penetration through the PEO coatings. On the other hand, the decrease in the current density and increases in the duty cycle and frequency lead to further reduction of the nanoparticles' incorporation and distribution on the coating surface.

DOI: 10.1007/s11661-017-4205-8


## I. INTRODUCTION

THE aluminum (Al) alloys are being utilized in widespread applications such as aerospace and other vital industries. Considerable corrosion resistance and high strength-to-weight ratio have made them suitable alloys for varied applications.[1,2] In comparison with other metals and alloys, Al and its alloys exhibit higher corrosion/oxidation resistance. The passive and hard film of Al oxide can impart wear/corrosion resistance and also protection.[3] The oxide film formation and quality can be improved electrochemically, using various appropriate electrolytes and applying different electrolysis treatments like the anodizing and the PEO on light alloys such as Al, Ti, and Mg. By the PEO treatment, using a specific electrolyte as the oxidizing environment, an oxide ceramic coating can be formed on the surface of light alloy, by applying potential higher than the dielectric breakdown potential.[4,5]

Many variables affecting the properties of the PEO-treated alloy are as follows: electrolyte's composition and temperature, applied voltage, current density, duration of treatment, alloy composition, *etc*. Recently, some electrolyte additives including silicate, aluminate, phosphate, and tungstate salts; micropowders; and nanoparticles (nps) have been investigated as the factors with effects on the properties of PEO-treated specimens.[6–14] Nanoparticle additives notably change the mechanical, tribological, electrochemical, and corrosion properties of the PEO-treated alloys. As revealed by this study, nanoparticles' incorporation on the coating during the growth process results in significant improvement in the coating's microstructure, morphology, thickness, and composition, and therefore, fundamental impact on the surface properties.[15–17] Moreover, the coating microstructure, morphology, thickness, and composition can be changed and improved by the PEO treatment, with the application of different levels of electrical parameters controlling the spark's discharge intensity and duration that are dependent on the energy and pulse-on time duration.[18,19] The variations in duty cycle, frequency, and current density alter the energy and pulse-on duration and so, define the surface discharge characteristics. These parameters influence

MOJTABA VAKILI-AZGHANDI and ARASH FATTAH-ALHOSSEINI are with the Department of Materials Engineering, Bu-Ali Sina University, Hamedan 65178-38695, Iran. Contact e-mail: m.vakiliazghandi92@basu.ac.ir
Manuscript submitted February 16, 2017.



Published online: 10 July 2017

the growth rate, microstructure, chemical analysis, and phase composition of the PEO coatings.[4,10] Accordingly, the PEO coating porosity, thickness, and composition are improved by the electrolyte compound's incorporation on the coating and the spark's discharge intensity and duration.

Many investigations have been conducted on how the application of different levels of electrical parameters and impact of various nps on the PEO coating's microstructure and other properties. Some studies have revealed the benefits of electrolyte np additives to different properties of the PEO coatings. Matykina *et al.*[10] found out that the suspension of the zirconia nps used in phosphate and silicate PEO electrolyte has been located on the coating surfaces and in cavities within the coatings on the Al substrate. Yürektürk *et al.*[11] studied the PEO coating formed on the 6082 aluminum alloy surface in aluminate PEO electrolyte containing carbon nanotubes. They found that the PEO process using an electrolyte containing CNT improves dry sliding wear resistance and surface hardness. Ma *et al.*[12] proposed the formation of a less-porous and denser oxide coating with lower friction coefficient by adding the graphite grains to the PEO electrolyte on the 6061 Al alloy. Sarbishei *et al.*[13] discovered that the amount of $Al_2O_3$ nps codeposited on the coating and the cavities formed by discharge channels are the major challenging factors controlling the PEO coating's thickness and porosity. Wang *et al.*[14] improved the anticorrosion property of the PEO coatings on AZ91D Mg alloy by adding the $Al_2O_3$ nps to the aluminate PEO electrolyte, which led to the formation of $MgAl_2O_4$ in the coating. Wang *et al.*[6] evaluated the effects of $Al_2O_3$ micropowder additives on corrosion behavior, microhardness, and PEO-treated samples' microstructure. They reported the increase in microhardness and corrosion current density as a result of the incorporation of $Al_2O_3$ micropowder on the coating during the coating growth process. Li *et al.*[20] undertook a research on the PEO-treated 6063 Al alloy specimens produced using the calumniate electrolyte containing $\alpha$-$Al_2O_3$ with a different current density. This led to the enhancement of surface topography and microhardness of PEO coating. Dehnavi *et al.*[21] investigated the effects of duty cycle, current density, and frequency on the microstructure and morphology of PEO-treated Al alloy specimens. They reported that decline in frequency and also increases in both current density and duty cycle, all of which result in reduction of the crater radius, increase in the coating's thickness, and the improvement of the silicon adsorption content on the surface. Yerokhin's *et al.*[22] experimental results revealed the effect of pulsed bipolar current on properties of the PEO-treated Al substrate. They explained that the growth rate and the ceramic coating's thickness have been increased and the volume fraction of the porous outer layer has been reduced by increasing the frequency. Guangliang's *et al.*[23] study explained that when the current density is lower than 10 $A/cm^2$, the PEO-treated samples consist mainly of $\gamma$-$Al_2O_3$, while the PEO-treated samples at higher current density are almost composed of $\alpha$-$Al_2O_3$.

As a result, still there is a lack of reliable knowledge about the effects of electrical parameters such as applied current density, duty cycle, and frequency on the np incorporation that can influence the electrochemical and corrosion properties of the PEO-treated Al alloy. These impacts are a result of enhancement in morphology and microstructure of the ceramic coating. In the previous study, we considered the effects of KOH, $Na_2SiO_3$, and $Al_2O_3$ np concentrations on the microstructural and corrosion properties of the PEO-treated Al alloy. Moreover, we optimized alkaline silicate electrolyte containing $Al_2O_3$ nps to improve the corrosion behavior of the PEO-treated Al alloy.[24,25]

In this study, we investigated the PEO treatment of 6061 Al alloy in the optimized alkaline silicate electrolyte both in the absence of and in the presence of $Al_2O_3$ nps. The PEO coating was applied at different levels of electrical parameters such as current density, frequency, and duty cycle, in order to observe the efficacy of the electrical parameters on the np incorporation, microstructure, morphology, and corrosion behavior of the PEO-treated 6061 Al alloy.

## II. EXPERIMENTAL PROCEDURES

The 6061 Al alloy plates, cut into pieces to the dimension 15 mm ×15 mm × 2 mm, were selected as the PEO samples. The chemical composition of the used 6061 Al alloy is illustrated in Table I. After grinding by 1200 grit emery paper, all samples were ultrasonically cleaned in acetone.

The silicate alkaline solution containing $Al_2O_3$ nps optimized in the previous study was applied as the components of the PEO electrolyte systems.[25] These electrolyte systems were composed of KOH 2 g $L^{-1}$, $Na_2SiO_3$ 5 g $L^{-1}$, and $Al_2O_3$ nps 3 g $L^{-1}$. In this study, we employed the optimized electrolyte with $Al_2O_3$ nps and also optimized electrolyte without $Al_2O_3$ nps.[25] The SEM and transmission electron microscopy (TEM) micrographs of $\alpha$-$Al_2O_3$ nps are illustrated in Figure 1. The PEO treatment was performed for 900 seconds at 303 K (30 °C) with different electrical parameters using IPC PM700/7 PRC AC/DC instrument in optimized silicate alkaline electrolyte with and without nanoparticles of $Al_2O_3$. During the process, the stainless steel hoop was utilized as a cathode, and the 6061 Al alloy sample was set as an anode. Anode and cathode were connected to a DC/AC power source. Various electrical

**Table I. Chemical Composition of 6061 Aluminum Alloy**

| Elements | Mg | Si | Fe | Cu | Cr | Ti | Al |
|---|---|---|---|---|---|---|---|
| 6061 Al alloy | 0.9 | 0.7 | 0.35 | 0.23 | 0.19 | 0.01 | bal. |

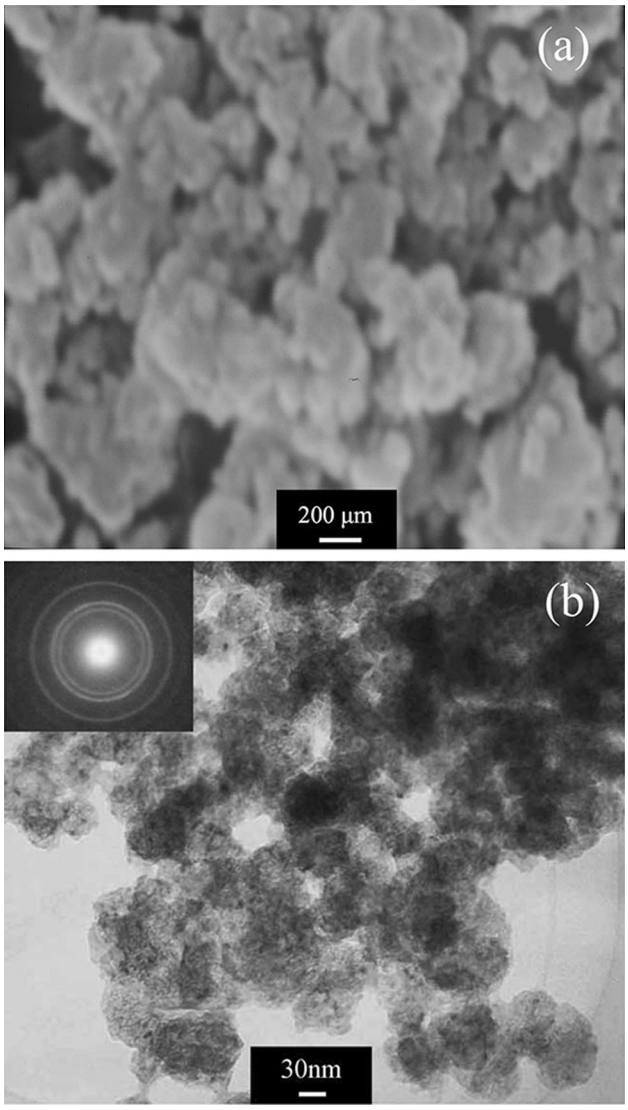


Fig. 1—(*a*) SEM micrograph and (*b*) TEM micrograph of $Al_2O_3$ nps, inset shows the selected area diffraction (SAD) pattern of particles.

parameters such as frequency, current density, and duty cycle in distinguishable applied ranges were used to study their influences on the PEO-coated microstructure and properties and also np incorporation. Table II illustrate two sample groups including A (PEOed with $Al_2O_3$ nps) and S (PEOed without $Al_2O_3$ nps).

In order to observe the surface morphology and microstructure of the PEO-treated samples, a JEOL JSM-840A SEM equipment was employed in two magnifications of 500X and 4000X. An Italstructures model APD2000 diffractometer using $CuK_\alpha$ radiation with diffraction angle of $2\theta$ range from 10 to 80 deg was utilized for XRD analysis and to analyze phases of the PEO-treated and untreated samples.

The corrosion and electrochemical behaviors of all PEO-treated samples were demonstrated by $\mu$Autolab Type III/FRA2 potentiostat system using a three-electrode lab flat cell. The corrosion medium was 3.5 wt pct NaCl electrolyte as a simulated seawater solution, pH = 7. The

**Table II. Different Electrical Conditions Used for PEO Treatment of 6061 Al Alloy Samples**

| Samples | Duty Cycle (Pct) | Current Frequency (Hz) | Current Density (A/dm$^2$) |
|---|---|---|---|
| S2-1-10* | 20 | 100 | 10 |
| A2-1-10 | | | |
| S8-1-10 | 80 | 100 | 10 |
| A8-1-10 | | | |
| S2-2-10 | 20 | 2000 | 10 |
| A2-2-10 | | | |
| S8-2-10 | 80 | 2000 | 10 |
| A8-2-10 | | | |
| S2-1-15 | 20 | 100 | 15 |
| A2-1-15 | | | |
| S8-1-15 | 80 | 100 | 15 |
| A8-1-15 | | | |
| S2-2-15 | 20 | 2000 | 15 |
| A2-2-15 | | | |
| S8-2-15 | 80 | 2000 | 15 |
| A8-2-15 | | | |

* The sample code was done as follows:
The first letters (S) and (A) refer to PEO treated samples in absence and presence of $Al_2O_3$ np.
The first numbers (2) and (8) refer to duty cycle 20 and 80 respectively.
The second numbers (1) and (2) refer to frequency 100 and 2000 Hz respectively.
The third numbers (10) and (15) refer to current density 10 and 15 A/dm$^2$ respectively.

reference electrode was Ag/AgCl (in saturated KCl solution), the PEO-treated samples were set as working electrodes, and platinum was defined as the auxiliary electrode. To reach the steady-state electrochemical condition, prior to the electrochemical tests, PEO-treated samples with an area of 0.4 cm$^2$ were exposed to the simulated seawater solution at 298 K (25 °C) for 7200 seconds [G3 −89 (Reapproved 2004)].

(a) DC electrochemical tests of PEO-treated samples were carried out by potentiodynamic polarization method from −0.25 V (*vs* open circuit potential) at a scan rate of 1 mVs$^{-1}$ to 0.5 V.

(b) AC electrochemical tests of PEO-treated samples were performed by electrochemical impedance spectroscopy (EIS) technique at the amplitude of 10 mV *vs* open circuit potential with a frequency range of 100 kHz to 0.01 mHz. Modeling, curve-fitting, and analysis of EIS data were done by EIS analyzer software.

## III. RESULTS AND DISCUSSION

### A. *SEM Observations*

Effects of the electrical parameters on the surface microstructures, morphologies, chemical composition and $Al_2O_3$ np incorporation in the PEO coatings formed using the electrolyte with and without $Al_2O_3$ nps on 6061 Al alloy, are presented in Figures 2 and 3. The SEM micrographs show the surface of PEO coatings formed at various frequency (100 and 2000 Hz) and duty cycle (20 and 80) in constant current densities equal to 10 and 15 A/cm$^2$ in Figures 2 and 3, respectively.

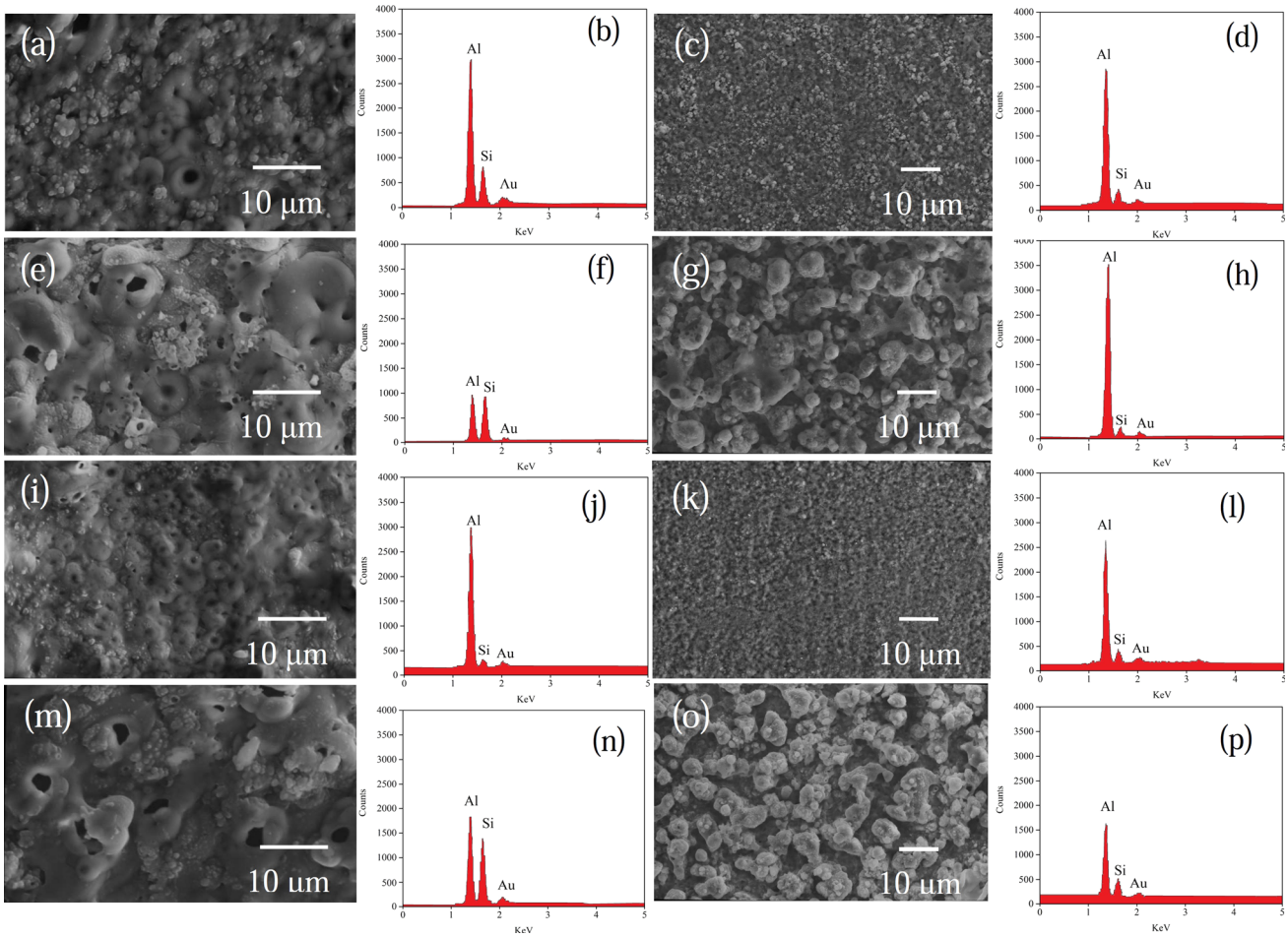


Fig. 2—SEM micrographs and EDS analysis of coating surfaces of samples (*a*, *b*) Sample S2-1-10, (*c*, *d*) Sample A2-1-10, (*e*, *f*) Sample S8-1-10, (*g*, *h*) Sample A8-1-10, (*i*, *j*) Sample S2-2-10, (*k*, *l*) Sample A2-2-10, (*m*, *n*) Sample S8-2-10, (*o*, *p*) Sample A8-2-10.

As can be seen, increasing the current density from 10 to 15 A/cm$^2$ under all different conditions with constant duty cycle and frequency, with $Al_2O_3$ nps and without $Al_2O_3$ nps, caused the relative increase in crater size. This can be attributed to the strong discharge as a result of increased growth rate of the coating and intensified microdischarges, and also lower spatial density of microdischarges in higher current density. All the PEO-coated samples with $Al_2O_3$ nps, have lower porosity compared to those without $Al_2O_3$ nps. The reason is the high incorporation and penetration of $Al_2O_3$ nps in the coating porosity through the PEO coating growth process. The surface characterization of the PEO-treated samples with $Al_2O_3$ nanoparticles with similar electrical parameters exhibited similar surface characteristic as shown in Figures 2(b), (d), (f) and (h) and also 3(b), (d), (f), and (h), respectively. Also, the surface characterization of the PEO-treated samples in the absence of $Al_2O_3$ nanoparticles using similar electrical parameters, showed similar surface characteristic. As can be seen in Figure 1(a) (SEM micrograph of $Al_2O_3$ nps) and Figures 2 and 3 (PEO-treated with $Al_2O_3$ nps and without them), it can be concluded that when we have $Al_2O_3$ nps, in spite of high concentration of $Na_2SiO_3$ in PEO electrolyte, the PEO-treated samples are covered by $Al_2O_3$ nps. It is revealed that the incorporation of $Al_2O_3$ nanoparticles is higher than that of Si ions. The analysis and study of surface topography proved that rise in the applied current density under all different conditions with constant frequency and duty cycle, could increase the penetration and the incorporation of $Al_2O_3$ nps in the PEO coatings in electrolytes creating a smoother surface, though there were intensified microdischarges in higher current density. The mentioned result can be attributed to the stronger electrical field established between the cathode and anode poles and also higher incorporation and penetration of $Al_2O_3$ nps on the molten aluminum, flowing out through discharge channels by increasing the current density.[5,14,15,18,22]

The effects of electrical parameters on distribution of elements in the coatings were studied by assessing the silicon per aluminum count ratio ($C_{Si}/C_{Al}$) extracted from EDS analysis of craters around the discharge channels, which are the oxidation and adsorption sites of the PEO coating surfaces. All the ($C_{Si}/C_{Al}$) ratios obtained from the EDS analyses are illustrated in Table III. As seen in the table, the $C_{Si}/C_{Al}$ ratio decreased in all the PEO-treated samples with $Al_2O_3$ nps compared to those without $Al_2O_3$ nps. This is related to $Al_2O_3$ np incorporation and also more

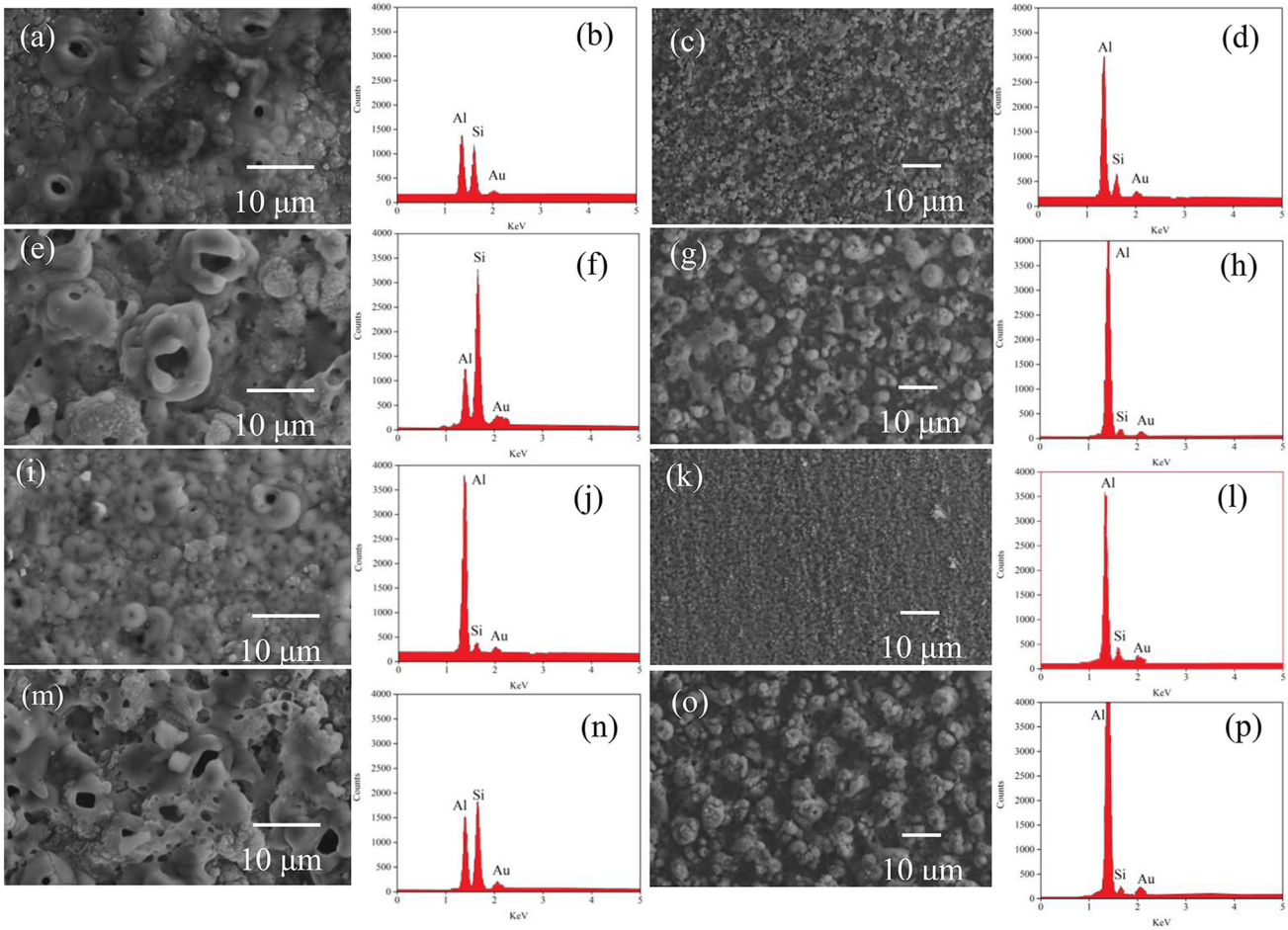


Fig. 3—SEM micrographs and EDS analysis of coating surfaces of samples (*a*, *b*) Sample S2-1-15, (*c*, *d*) Sample A2-1-15, (*e*, *f*) Sample S8-1-15, (*g*, *h*) Sample A8-1-15, (*i*, *j*) Sample S2-2-15, (*k*, *l*) Sample A2-2-15, (*m*, *n*) Sample S8-2-15, (*o*, *p*) Sample A8-2-15.

**Table III. Silicon Per Aluminum Count Ratio ($C_{Si}/C_{Al}$) of PEO-treated 6061 Aluminum Alloy in Different Electrical Parameters as EDX Analysis**

| Samples | S2-1-10 | S8-1-10 | S2-2-10 | S8-2-10 | S2-1-15 | S8-1-15 | S2-2-15 | S8-2-15 |
|---|---|---|---|---|---|---|---|---|
| $C_{Si}/C_{Al}$ | 0.256 | 0.959 | 0.179 | 0.777 | 0.869 | 2.670 | 0.263 | 1.215 |
| Samples | A2-1-10 | A8-1-10 | A2-2-10 | A8-2-10 | A2-1-15 | A8-1-15 | A2-2-15 | A8-2-15 |
| $C_{Si}/C_{Al}$ | 0.122 | 0.059 | 0.134 | 0.062 | 0.076 | 0.036 | 0.097 | 0.046 |

incorporation of $Al_2O_3$ nps compared with Si-containing spices duration the PEO treatment.

This analysis and study of $C_{Si}/C_{Al}$ ratio showed that increase in the applied current density under all different conditions with constant duty cycle and frequency caused decrease and increase in the $C_{Si}/C_{Al}$ ratio in the presence and the absence of $Al_2O_3$ nps, respectively. This is attributed to the increase in penetration and incorporation of Si and $Al_2O_3$ nps during the PEO treatment. The more incorporation of Si and $Al_2O_3$ nps can be related to lower spark density produced by higher current density, creating the lower number of sparks on the surface. The lower number of sparks on the surface can increase the craters around the discharge channels, which are the oxidation and adsorption sites of the PEO coating surfaces. As a result, $Al_2O_3$ nps and Si spices become detached from the surface of the coatings by decreasing the applied current density.[5,14,15,18,22]

The effects of increasing duty cycle from 20 to 80 under all different conditions with constant frequency and the impact of applied current density, on the microstructure, morphology and $Al_2O_3$ nps are presented in Figures 2 and 3. As can be seen, the size of the craters is augmented in the PEO-coated samples processed with duty cycle equal to 80 compared to the one treated by duty cycle of 20, using solutions in the presence of $Al_2O_3$ nps and in the absence of them. Since the total duration of a pulse on time in the constant

current density and frequency is higher in greater duty cycle, the overall input power increases with the increasing duty cycle. As a result, an increment in the duty cycle caused the creation of a stronger microdischarge, greater crater size, and lower spatial density. The SEM micrographs showed that the coating porosity increased by adding the duty cycle. This can be attributed to higher duty cycles producing microdischarges with lower spatial density and higher intensity. In addition, higher duty cycles improved the chance of trapping dissolved oxygen in larger microdischarges and craters. Paying attention to the surface topography of the PEO-coated specimens in different duty cycles with constant frequency and applied current density proved that the $Al_2O_3$ np distribution in the PEO-treated samples have more homogeny in lower duty cycle. On the other hand, due to the higher intensity and lower spatial density of microdischarges in higher duty cycle, incorporation and penetration of $Al_2O_3$ nps in duty cycle of 80 were higher in comparison with the duty cycle equal to 20. Additionally, higher spark density produced by lower duty cycle, creates the larger number of sparks on the surface. As a result, $Al_2O_3$ nps become detached from the surface of the coatings provided by the solutions containing $Al_2O_3$ nps. Moreover, duration of a pulse on time related to the higher duty cycle, causes more surface remelting and further incorporation and penetration of $Al_2O_3$ nps on the PEO coating.[13,19,23–27] The study of $C_{Si}/C_{Al}$ ratio showed that increase in the duty cycle under all different conditions with constant current density and frequency caused decrease and increase in the $C_{Si}/C_{Al}$ ratio in the presence and the absence of $Al_2O_3$ nps, respectively (Table III). This is attributed to the increase in penetration and incorporation of Si and $Al_2O_3$ nps during the PEO treatment. The more incorporation of Si and $Al_2O_3$ nps can be attributed to the lower spark density produced by higher duty cycle, creating the lower number of sparks on the surface.[13,19,23–27]

Figures 2 and 3 are illustrating the effects of different applied frequencies (100 and 2000 Hz) under various conditions with constant duty cycle and applied current density on the microstructure and morphology of the surface, and also on the $Al_2O_3$ np incorporation during the PEO process. The surface micrographs displayed partly increased porosity and crater size as a result of decline in the applied frequency during the PEO process with and without nanoparticles of $Al_2O_3$ in the electrolyte. This can be attributed to the impact of frequency on duration of the pulse on and pulse off time. The higher frequency in comparison with the lower one, results in lower duration of one single pulse, providing finer microdischarge.[28–30] Consequently, a lower duration of one single pulse is the reason of lower discharge intensity, reduced porosity and decreased crater size. This consequence is more visible in lower duty cycle, since there is a lower pulse on time in comparison with the application of the higher duty cycle. The surface characterization showed reduction of $Al_2O_3$ nps in current frequency of 2000 Hz compared with the frequency of 100 Hz. Furthermore, the $Al_2O_3$ np distribution has more homogeny in the PEO-treated samples in higher frequency. High spark density produces a larger number of sparks on the surface and that is why the $Al_2O_3$ nps are detached from the surface.[19,23,24,27–30] The study of $C_{Si}/C_{Al}$ ratio showed that increase in the current frequency under all different conditions with constant current density and duty cycle caused increase and decrease in the $C_{Si}/C_{Al}$ ratio in the presence and the absence of $Al_2O_3$ nps, respectively (Table III). This is attributed to the decrease in penetration and incorporation of Si and $Al_2O_3$ nps during the PEO treatment by increasing current frequency. The lower incorporation of Si and $Al_2O_3$ nps can be related to the higher spark density produced by higher current frequency, creating the higher number of sparks on the surface. As a result, $Al_2O_3$ nps and Si spices become detached from the surface of the coatings by increasing the applied current frequency.[19,23,24,27–30]

### B. *Phase Analyses*

The XRD pattern of 6061 Al alloy and PEO-treated sample using the solution with $Al_2O_3$ nps and without them, are presented in Figure 4. The intense diffraction peaks of the aluminum were detected in treated and untreated samples. Since the coatings were so thin and porous, the X-rays could easily penetrate through the substrate. Al peaks intensity was reduced in the PEO-treated samples compared with Al substrate. This is related to different phase formation on the Al substrate during the PEO treatment. Different phases can be analyzed in the PEO-treated samples. Comparing the phases of the PEO-treated samples with untreated ones, one could conclude that the PEO coatings are composed of mullite ($3Al_2O_3.2SiO_2$), $\alpha$-$Al_2O_3$ and $\gamma$-$Al_2O_3$. The mullite phase is an important ceramic phase characterized by acceptable chemical and thermal stability, the $\alpha$-$Al_2O_3$ phase is a stable alumina with a high melting point [2323 K (2050 °C)], and $\gamma$-$Al_2O_3$ phase is a metastable alumina phase which can be transformed into $\alpha$-$Al_2O_3$ by heating in a temperature

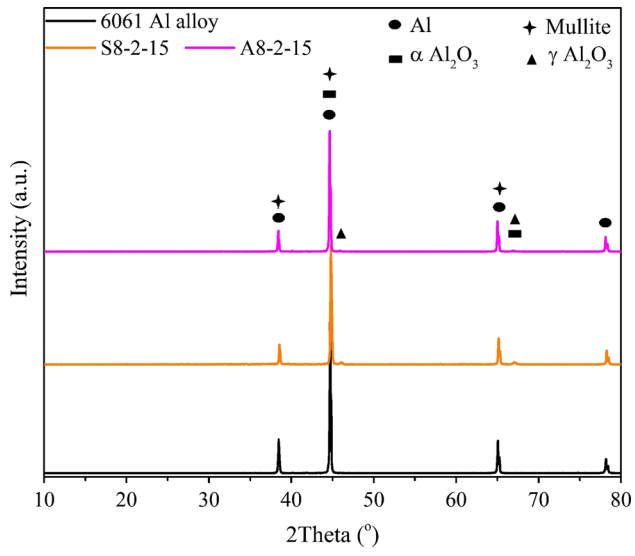


Fig. 4—XRD pattern of untreated and PEO-treated 6061 Al alloy samples in the absence and the presence of $Al_2O_3$ nps.

range between 1073 K and 1473 K (800 °C and 1200 °C).[17,31–41]

As seen, compared with the untreated samples, the aluminum peaks' intensities have been reduced in PEO-treated specimens. This can be related to the X-ray adsorption by different phases formed on the aluminum substrate due to the PEO treatment. Accordingly, the $\alpha$-$Al_2O_3$ peaks' intensities have been increased in PEO-treated sample in the presence of $Al_2O_3$ nps, compared with the specimen without it. Here, the incorporation and penetration of $Al_2O_3$ nps on the PEO coating induce the difference. As seen, the intensities of the $\gamma$-$Al_2O_3$ diffraction peaks have been reduced in the sample A8-2-15 compared with sample S8-2-15, due to the $\alpha$-$Al_2O_3$ np incorporation.

### C. *Potentiodynamic Polarization Measurements*

Corrosion and electrochemical behavior of the PEO coatings formed on the 6061 Al plate in PEO electrolyte with and without $Al_2O_3$ nps using different electrical parameters were tested by potentiodynamic polarization technique as a DC test. The potentiodynamic polarization curves including the anodic and cathodic branches in applied current density of 10 and 15 A $cm^{-2}$ are presented in Figures 5 and 6, respectively. All of the anodic branches of different PEO-treated samples in the presence of $Al_2O_3$ nps and in the absence of them, presented three regions including active polarization region, passivation region, and breakdown region. At first, the active polarization region, increasing the anodic potential, sharply adds to the current density.

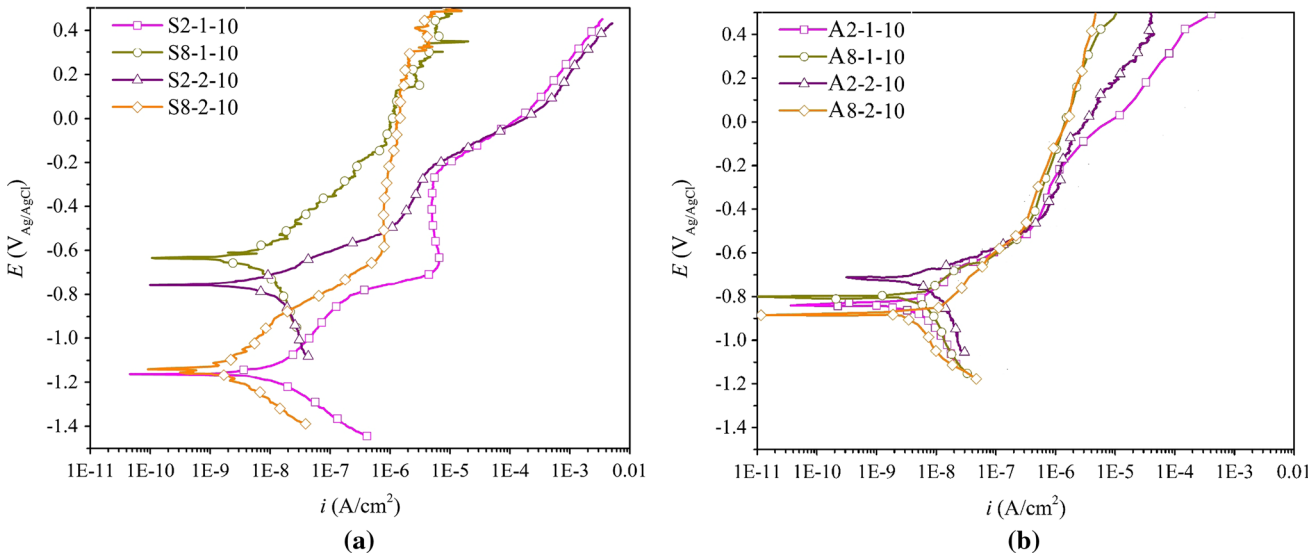


Fig. 5—Polarization curves of PEO-treated samples in applied current density equal to 10 A/$cm^2$: (*a*) in PEO electrolyte without $Al_2O_3$ nps, and (*b*) in PEO electrolyte with $Al_2O_3$ nps.

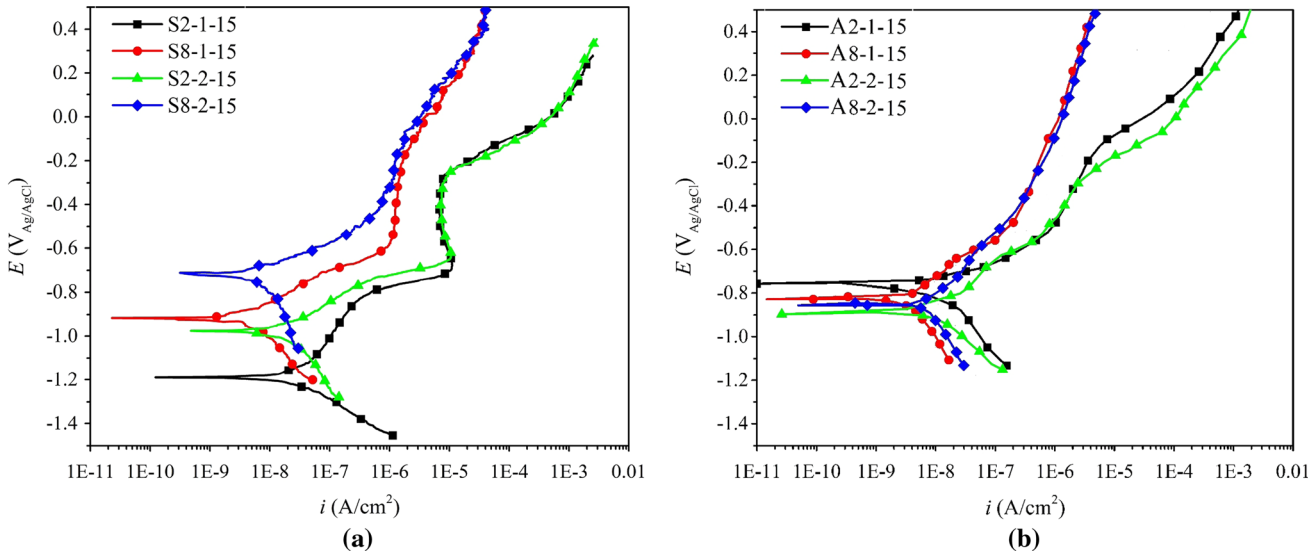


Fig. 6—Potentiodynamic polarization curves of PEO-treated samples in applied current density equal to 15 A/$cm^2$: (*a*) in PEO electrolyte without $Al_2O_3$ nps, and (*b*) in PEO electrolyte with $Al_2O_3$ nps.

This proves that anodic process is controlled by the activation polarization. Next, the passivation region demonstrates that with increasing the applied anodic potential, current density have become stable or constant. This is due to the high corrosion/oxidation resistance of the oxide ceramic layer formed on the 6061 Al plate by the PEO treatment. The final region on the anodic branches exhibited that sharp increment in current density is the result of increasing the applied anodic potential. This can be referred to the annihilation of the ceramic coating by detachment, or pitting occurrence throughout coating at high applied anodic potential. All cathodic branches appeared in the active region, showed that the cathodic process is controlled by the activation polarization. The extrapolation of the Tafel slope at open circuit potential gives the corrosion potential and the corrosion current density in each polarization curve of the PEO-treated samples. Also, corrosion current density in the passivation region, illustrated as oxide corrosion current density, explains that increasing the anodic potential, slightly increases the current density.[42,43] All the extracted data from potentiodynamic polarization curves of the PEO-treated samples with and without nanoparticles of $Al_2O_3$ in different applied electrical parameters are available in Table IV. These parameters include corrosion potential ($E_{corr}$), corrosion current density ($i_{corr}$), and current density of the oxide layer ($i_{ox}$).

As can be seen, all the PEO-treated samples with $Al_2O_3$ nps illustrate lower corrosion current density and reduced current density of the oxide layer in comparison with the PEO-treated samples without $Al_2O_3$ nps under the same applied electrical conditions. As a result, in the presence of $Al_2O_3$ nps, coatings with lower porosity are formed. This can be attributed to the penetration and the incorporation of $Al_2O_3$ nps on melted surface of the PEO coating during the growth process. In addition, compared with the coatings without $Al_2O_3$ nps, higher positive values of potential are obtained in the coatings with nanoparticles of $Al_2O_3$. This confirms the penetration and the incorporation of $Al_2O_3$ nps throughout the oxide coating formed on the 6061 Al alloy. The effect of different applied current density on the potentiodynamic polarization curves of the PEO-treated samples reveals that current density of the oxide layer and also corrosion current density of different PEO-treated samples with and without using $Al_2O_3$ nps are reduced when the applied current density decreases at constant duty cycle in the PEO treatment, and the current frequency increases. The samples S2-1-15, S8-1-15, S2-2-15 and S2-2-15 and also A2-1-15, A8-1-15, A2-2-15 and A2-2-15 displayed higher corrosion current density than specimens S2-1-10, S8-1-10, S2-2-10 and S2-2-10 and also A2-1-10, A8-1-10, A2-2-10 and A2-2-10, respectively. This is due to improvement in the coating growth mechanism and decrease in the coating growth rate in lower applied current density as discussed in the last section.

**Table IV. Potentiodynamic Polarization Parameters for Treated 6061 Al Alloy Under Different Electrical Parameters**

| Samples | $i_{corr}$ ($\mu$A/cm$^2$) | $E_{corr}$ ($V$ *vs* Ag/AgCl) | $i_{OX}$ ($\mu$A/cm$^2$) |
|---|---|---|---|
| S2-1-10 | 8.2 | −1.171 | 5.34 |
| A2-1-10 | 5.7 | −0.852 | 0.82 |
| S8-1-10 | 4.5 | −0.638 | 0.24 |
| A8-1-10 | 2.8 | −0.733 | 0.19 |
| S2-2-10 | 6.5 | −0.758 | 2.22 |
| A2-2-10 | 4.4 | −0.714 | 1.26 |
| S8-2-10 | 1.5 | −1.121 | 0.84 |
| A8-2-10 | 3.4 | −0.865 | 0.29 |
| S2-1-15 | 18.1 | −1.189 | 6.42 |
| A2-1-15 | 8.4 | −0.831 | 3.31 |
| S8-1-15 | 5.5 | −0.911 | 1.21 |
| A8-1-15 | 4.7 | −0.828 | 0.51 |
| S2-2-15 | 11.2 | −0.974 | 7.72 |
| A2-2-15 | 7.2 | −0.856 | 1.58 |
| S8-2-15 | 4.1 | −0.702 | 1.12 |
| A8-2-15 | 4.5 | −0.843 | 0.26 |

The influence of two levels of duty cycle in different current density and frequency on corrosion and electrochemical behavior of the PEO-treated samples, with or without $Al_2O_3$ nps, was investigated by the potentiodynamic polarization test. As can be found in Table IV, with increase in duty cycle, the current density of the oxide layer and the corrosion current density have been dropped. In addition, with increasing duty cycle, the corrosion potential has been shifted to a positive value indicating a nobler behavior of the PEO-treated samples. This is due to the higher incorporation and penetration of $Al_2O_3$ nps and also other dispersed species in the coating at high duty cycle, increasing the coating thickness and decreasing the PEO coating microstructural defects (decreasing the PEO coating is explained in the EIS section).

The applied current frequency as an influential electrical parameter on the microstructure, morphology and coating growth rate and mechanism, can affect the corrosion and electrochemical behavior of the PEO-treated samples with and without $Al_2O_3$ nps. As can be seen in Figures 5, 6 and Table IV, with increasing the current frequency from 100 to 2000 Hz, the current density of the oxide layer and also corrosion current density have been decreased. The reason is reduction in the PEO coating crater size and porosity.

Finally, the PEO-treated samples under conditions of high applied current density (15 A/cm$^2$), high duty cycle (80), and increased current frequency (2000 Hz)—in comparison with the PEO-treated samples under low applied current density (10 A/cm$^2$), low duty cycle (20), and decreased current frequency (100 Hz)—illustrated better corrosion behavior with lower corrosion current density and reduced current density of the oxide layer.

### D. *EIS Measurements*

EIS is one of the AC electrochemical tests for analyzing the properties of the charge-transfer mechanism at the electrolyte/ electrode interface and to determine the electrical properties and corrosion resistances of different layers formed on the substrate during the PEO treatment.[44,45] The EIS plots including Nyquist, Bode phase and Bode module diagrams of

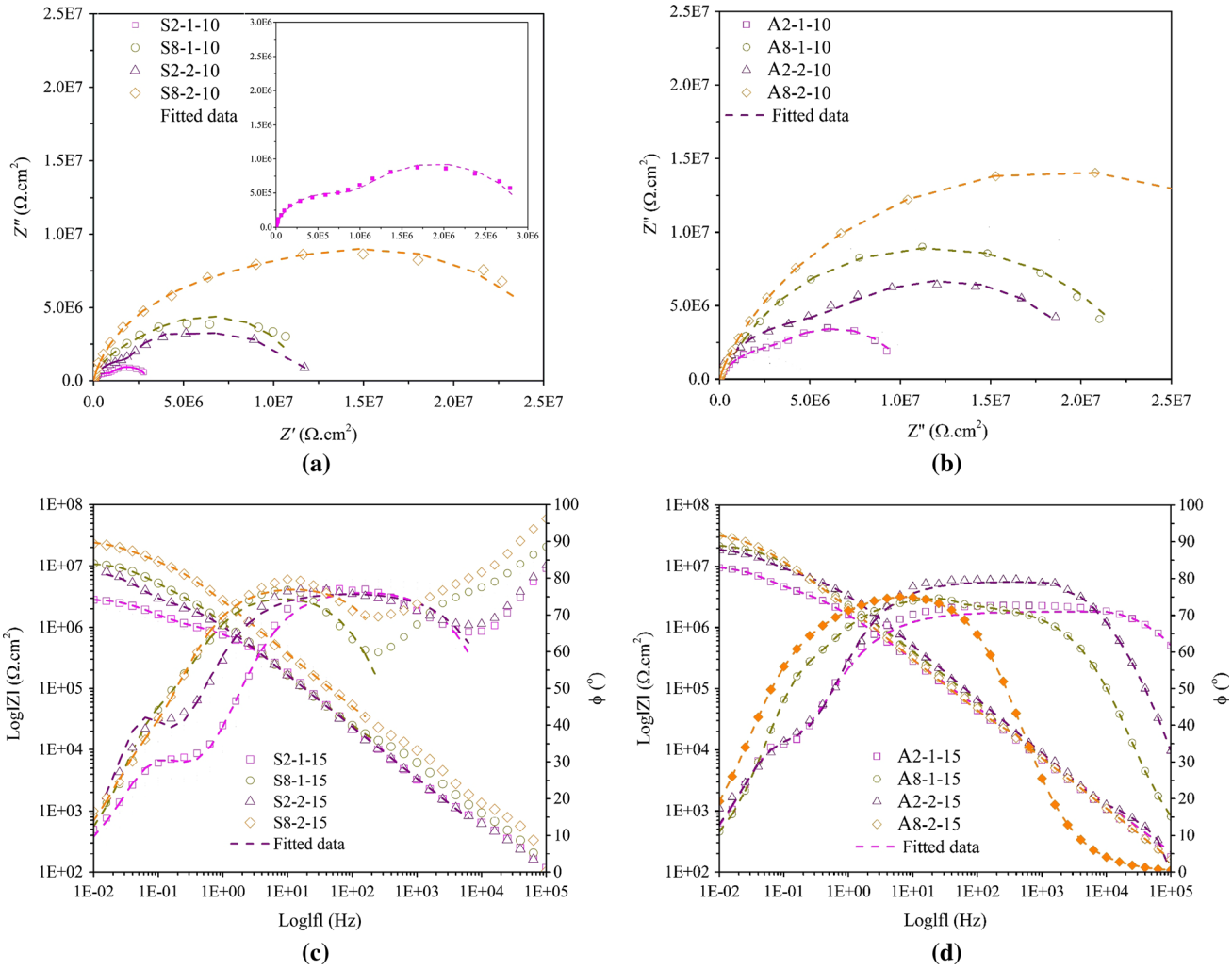


Fig. 7—Nyquist and Bode phase plots of PEO-treated samples at an applied current density of 10 A/cm$^2$: (*a*, *c*) in PEO electrolyte without $Al_2O_3$ nps, and (*b*, *d*) in PEO electrolyte with $Al_2O_3$ nps.

different PEO coatings formed in current density of 10 A.cm$^{-2}$ and 15 A.cm$^{-2}$ in the simulated seawater solution are presented in Figures 7 and 8, respectively. EIS measurements can be analyzed and simulated by an equivalent electrical circuit shown in Figure 9. All diagrams have presented two-time constants at the low and high applied frequencies. This behavior is due to the performance characteristics of two layers: the outer porous oxide film as a functional layer, and the inner dense layer as a barrier. Therefore, different applied electrical parameters caused the formation of PEO coatings with similar EIS curves but with different capacitance and resistance values. In this equivalent electrical circuit, *Rs* refers to solution resistance, $R_{out}$ and $R_{in}$ stand for the functional (outer) and the barrier (inner) resistance layers, and $CPE_{out}$ and $CPE_{in}$ refer to the constant phase elements of the functional and barrier layers, respectively.

The impedance of CPE ($Z_{CPE}$) denoting the incomplete capacitance of each layer can be formulated by Eq. [1][44–46]:

$$Z_{CPE}[Q(j\omega^n)]^{-1}, \quad [1]$$

where *j*, *Q*, $\omega$, and *n* represent the imaginary unit, the CPE constant, the angular frequency (rad/s), and the exponent of CPE, respectively.

All the extracted EIS data by the equivalent electrical circuit are illustrated in Table V. As comprehended from the table, the charge-transfer capacitance of barrier layers is more than that of the functional layer in all the PEO-treated samples with $Al_2O_3$ nps and without $Al_2O_3$ nps. According to the Eq. [3], this may be related to the decrease in the dielectric constant of the barrier layer compared with a functional layer formed with lower structural defects and porosity. The mentioned conclusion is attributed to the lower coating growth rate in the barrier layer. Moreover, the $R_{out}$, $R_{in}$, and $R_p$ (*i.e.* $R_{out} + R_{in}$) of all PEO-treated samples with $Al_2O_3$ nps, are higher than those of all PEO-treated samples without $Al_2O_3$ nps. On the other hand, compared with the specimens without $Al_2O_3$ nps, the PEO-treated samples with nanoparticles of $Al_2O_3$

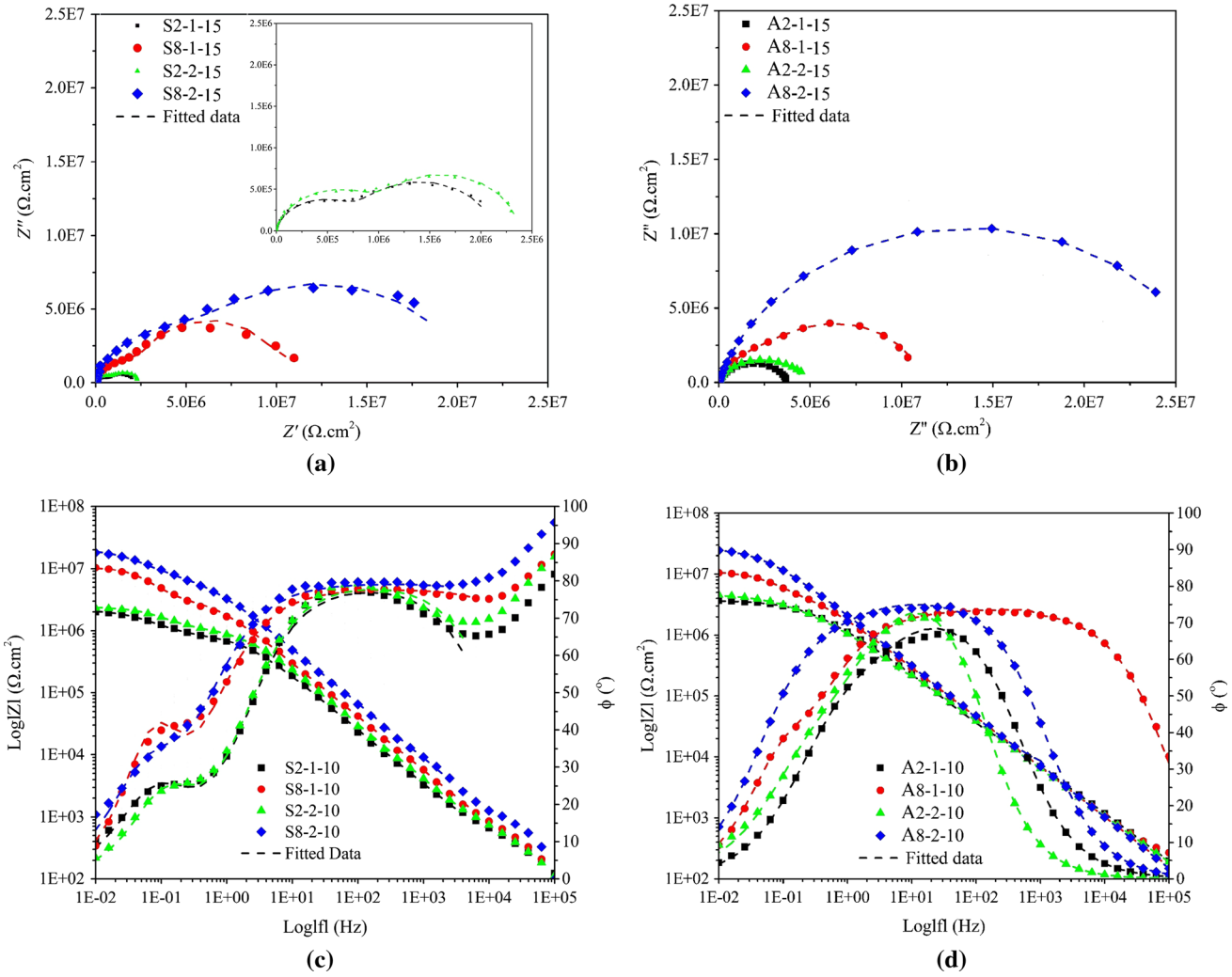


Fig. 8—Nyquist and Bode phase plots of PEO-treated samples at an applied current density of 15 A/cm$^2$: (*a*, *c*) in PEO electrolyte without $Al_2O_3$ nps, and (*b*, *d*) in PEO electrolyte with $Al_2O_3$ nps.

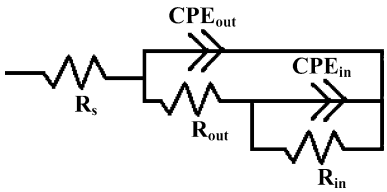


Fig. 9—The equivalent electrical circuit used to fit the impedance data of PEO-treated samples.

present lower charge-transfer capacity. These results can be attributed to the increase in the coating thickness, higher coating density, reduced porosity, and decline in the structural defects. All the described factors decreasing the electrical constant are a consequence of the incorporation and penetration of $Al_2O_3$ nps on the PEO coating during the growth process. The charge-transfer capacity ($C_L$), calculated by Eq. [2] has been reduced with the increasing corrosion resistance[43–49]:

$$C_L = Q^{-1} R_L^{1-n/n}, \quad [2]$$

where $Q$, $n$, and $R$ are the constant-phase element parameter, deviation parameter, and resistance of layers on 6061 Aluminum alloy, respectively.

Considering Eq. [3], charge-transfer capacity reductions of different layers formed by PEO treatment confirm the decrease in the local dielectric constant, or the increment in the coating thickness[43–49]:

$$C_L = \frac{\varepsilon \varepsilon_0}{d} S, \quad [3]$$

where $\varepsilon$ is the local dielectric constant, $\varepsilon_0$ represents the permittivity of the air, $d$ is the thickness of the layer, and $S$ stands for the surface area of the electrode. The effects of the applied current density, duty cycle, and frequency on the corrosion behavior of the PEO-treated samples with and without $Al_2O_3$ nps are depicted in Figures 7, 8, and Table V. The illustrated results show that increasing the applied current density decreases $R_{out}$, $R_{in}$, and $R_p$ representing the $R_{out} + R_{in}$. The greater $R_p$ value

Table V. EIS Parameters for PEO-Treated 6061 Al Alloy with Different Electrical Parameters

| Samples | $R_s$ ($\Omega$ cm$^2$) | $R_{out}$ (M$\Omega$ cm$^2$) | $R_{in}$ (M$\Omega$ cm$^2$) | $R_P$ (M$\Omega$ cm$^2$) | $C_1$ ($\mu$F cm$^{-2}$) | $C_2$ ($\mu$F cm$^{-2}$) |
|---|---|---|---|---|---|---|
| S2-1-10 | 248 | 1.15 | 1.87 | 3.02 | 0.341 | 4.619 |
| A2-1-10 | 142 | 5.56 | 4.85 | 10.41 | 0.151 | 0.744 |
| S8-1-10 | 5785 | 6.71 | 4.78 | 11.50 | 0.475 | 0.383 |
| A8-1-10 | 156 | 9.82 | 13.92 | 23.753 | 0.113 | 0.083 |
| S2-2-10 | 210 | 5.71 | 6.85 | 12.56 | 0.403 | 1.100 |
| A2-2-10 | 63 | 8.71 | 12.31 | 21.02 | 0.131 | 0.893 |
| S8-2-10 | 591 | 10.08 | 16.23 | 26.28 | 1.191 | 1.185 |
| A8-2-10 | 217 | 13.51 | 23.84 | 27.35 | 0.112 | 0.059 |
| S2-1-15 | 354 | 0.80 | 1.24 | 2.13 | 0.291 | 6.936 |
| A2-1-15 | 336 | 1.39 | 2.64 | 4.03 | 0.112 | 0.482 |
| S8-1-15 | 70 | 3.65 | 6.86 | 10.51 | 0.213 | 1.154 |
| A8-1-15 | 245 | 0.84 | 6.38 | 7.22 | 0.132 | 0.403 |
| S2-2-15 | 338 | 1.15 | 1.21 | 2.37 | 0.230 | 4.261 |
| A2-2-15 | 156 | 1.53 | 3.18 | 4.71 | 0.122 | 0.496 |
| S8-2-15 | 64 | 8.37 | 12.12 | 20.49 | 0.127 | 0.904 |
| A8-2-15 | 148 | 12.78 | 14.49 | 27.27 | 0.109 | 0.071 |

corroborates the improvement in the corrosion-resistance behavior of the PEO-treated samples with and without $Al_2O_3$ nps. This can be better explained by the improvement in the coating growth mechanism and the decrease in the coating growth rate at lower applied current density as discussed in the previous section.

The effects of duty cycle on the electrochemical resistance and charge-transfer properties of the PEO-treated samples were investigated by the EIS technique. All the PEO-treated samples exhibiting similar Nyquist, Bode module, and Bode phase plots are showing two layers formed on the aluminum alloy by the PEO treatment at different applied duty cycles. Here, at a duty cycle of 80 in comparison with the duty cycle of 20, the corrosion resistance ($R_p$) increased, and the charge-transfer capacity declined. Considering the Eq. [3], improvement of the corrosion behavior can be related to the decreased electrical constant. This can be better explained by the higher incorporation of dispersed particles during the coating's growth process at higher duty cycle.

Corrosion-resistance and charge-transfer behaviors of the PEO-treated samples at various applied current frequencies evaluated by the EIS test showed different corrosion-resistance and charge-transfer capacity values with similar charge-transfer mechanism. The increase in the corrosion resistance and the reduction in the charge-transfer capacity in the PEO coating formed at high-current frequency can be elucidated by their lower porosity and lower growth rate of the coating.

## IV. CONCLUSION

Different electrical parameters of a unipolar pulsed current were applied in the PEO process of 6061 Al alloy using alkaline silicate electrolyte with and without $Al_2O_3$ nanoparticles. The conclusions drawn from the current study are as follows:

1. Microstructural characterizations of the PEO coating formed in the absence of $Al_2O_3$ nps showed that increases in the current density and the duty cycle, and decrease in the frequency lead to PEO coating with larger porosity and greater craters as a result of the higher discharge intensity on the surface.
2. Corrosion behavior of the PEO coating formed in the presence and in the absence of $Al_2O_3$ nps showed that decrease in the current density and increases in the duty cycle and frequency lead to the PEO coating with lower corrosion rate in relation to their microstructures.
3. The incorporations of $Al_2O_3$ nps and Si spices were increased with the increasing current density and duty cycle, and with the decreasing current frequency, as a result of lower spatial density and higher microdischarge intensity.
4. All the PEO coatings formed with the incorporation of $Al_2O_3$ nps exhibited lower porosity and more compact microstructure in comparison with the specimens without the incorporation of nanoparticles of $Al_2O_3$. Such a result is due to the incorporation and penetration of nanoparticles during the growth process of PEO coating. Therefore, the PEO coatings incorporated with $Al_2O_3$ nps presented better corrosion behavior in comparison with their counterparts free of $Al_2O_3$ nps.
5. XRD patterns displayed that the PEO processes led to the formation of mullite phases, $\gamma$-$Al_2O_3$ and $\alpha$-$Al_2O_3$, on the aluminum substrate. The aluminum peaks' intensities were reduced in the PEO-treated samples compared with the untreated ones. This can be a result of X-ray adsorption by different phases formed on the aluminum substrate during the PEO treatment. Accordingly, due to the incorporation and penetration of $Al_2O_3$ nps, the $\alpha$-$Al_2O_3$ peaks' intensities increased, and those of the $\gamma$-$Al_2O_3$ peaks were declined in the PEO-treated samples incorporated with $Al_2O_3$ nps compared with the treated specimens without $Al_2O_3$ nps.

## REFERENCES


1. C. Grard: *Aluminium And Its Alloys*, Constabl and company LTD, Cambridge, 1920, pp. 2–9.
2. H. Of: *Analytical Characterization of Aluminium, Steel, and Superalloys*, Taylor and Francis Group, New York, 2006, pp. 4–17.
3. C. Vargel: *Corrosion of Aluminium*, Elsevier Ltd, Amsterdam, 2004, pp. 81–90.
4. N. Huang, Y.X. Leng, and P.D. Ding: *Surf. Eng. Light Alloy.*, 2010, vol. 40, pp. 83–178.
5. A.L. Yerokhin, X. Nie, A. Leyland, A. Matthews, and S.J. Dowey: *Surf. Coatings Technol.*, 1999, vol. 122, pp. 73–93.
6. P. Wang, T. Wu, Y.T. Xiao, J. Pu, X.Y. Guo, and J. Huang: *J. Mater. Eng. Perform.*, 2016, vol. 25, pp. 3972–76.
7. M. Sabaghi Joni and A. Fattah-alhosseini: *J. Alloy. Compd.*, 2016, vol. 661, pp. 237–44.
8. A. Fattah-alhosseini and M. Sabaghi: *Joni. J. Mater. Eng. Perform.*, 2015, vol. 24, pp. 3444–52.
9. Y. Liu, J. Xu, Y. Gao, Y. Yuan, and C. Gao: *Phys. Procedia.*, 2012, vol. 32, pp. 107–12.
10. E. Matykina, R. Arrabal, F. Monfort, P. Skeldon, and G.E. Thompson: *Appl. Surf. Sci.*, 2008, vol. 255, pp. 2830–39.
11. Y. Yürektürk, F. Muhaffel, and M. Baydoğan: *Surf. Coat. Technol.*, 2014, vol. 269, pp. 83–90.
12. K. Ma, M.M.S. Al, and W. Wu: *Surf. Coat. Technol.*, 2014, vol. 259, pp. 318–24.
13. S. Sarbishei, M.A. Faghihi Sani, and M.R. Mohammadi: *Vacuum*, 2014, vol. 108, pp. 12–19.
14. Y. Wang, D. Wei, J. Yu, and S. Di: *J. Mater. Sci. Technol.*, 2014, vol. 30, pp. 1–7.
15. S. Di, Y. Guo, H. Lv, and J. Yu: *Ceram. Int.*, 2014, vol. 41, pp. 6178–86.
16. C. Kim, J. Choi, H. Kim, D. Lee, C. Hyun, and S. Nam: *Ceram. Int.*, 2012, vol. 38, pp. 5621–27.
17. A. Bahramian, K. Raeissi, and A. Hakimizad: *Appl. Surf. Sci.*, 2015, vol. 351, pp. 13–26.
18. R.O. Hussein, D.O. Northwood, and X. Nie: *Surf. Coat. Technol.*, 2013, vol. 237, pp. 357–68.
19. A. Anders: *Surf. Coat. Technol.*, 2004, vol. 183, pp. 301–11.
20. H.X. Li, W.J. Li, R.G. Song, and Z.G. Ji: *Mater. Sci. Technol.*, 2012, vol. 28, pp. 565–68.
21. V. Dehnavi, B.L. Luan, D.W. Shoesmith, X.Y. Liu, and S. Rohani: *Surf. Coat. Technol.*, 2013, vol. 226, pp. 100–07.
22. A.L. Yerokhin, A. Shatrov, V. Samsonov, P. Shashkov, A. Pilkington, and A. Leyland: *Surf. Coat. Technol.*, 2005, vol. 199, pp. 150–57.
23. Y. Guangliang, L. Xianyi, B. Yizhen, C. Haifeng, and J. Zengsun: *J. Alloys Compd.*, 2002, vol. 345, pp. 196–200.
24. A. Fattah-alhosseini, M. Keshavarz, and K.M. Vakili-azghandi: *Acta Metall. Sin. (English Lett)*, 2016, vol. 29, pp. 274–81.
25. M. Vakili-Azghandi, A. Fattah-alhosseini, and M.K. Keshavarz: *J. Mater. Eng. Perform.*, 2016, vol. 25, pp. 5302–13.
26. Y. Ma, X. Nie, D.O. Northwood, and H. Hu: *Thin Solid Films.*, 2006, vol. 494, pp. 296–301.
27. X. Wu, P. Su, Z. Jiang, and S. Meng: *ACS Appl. Mater. Interfaces.*, 2010, vol. 2, pp. 808–12.
28. R.H.U. Khan, A. Yerokhin, X. Li, H. Dong, and A. Matthews: *Surf. Coat. Technol.*, 2010, vol. 205, pp. 1679–88.
29. Y. Vangolu, E. Arslan, Y. Totik, E. Demirci, and A. Alsaran: *Surf. Coat. Technol.*, 2010, vol. 205, pp. 1764–73.
30. M. Sandhyarani, M. Ashfaq, T. Arunnellaiappan, M.P. Selvan, S. Subramanian, and N. Rameshbabu: *Surf. Coat. Technol.*, 2015, vol. 269, pp. 286–94.
31. F. Jaspard-Mécuson, T. Czerwiec, G. Henrion, T. Belmonte, L. Dujardin, and A. Viola: *Surf. Coat. Technol.*, 2007, vol. 201, pp. 8677–82.
32. J. Wang, M. Du, F. Han, and J. Yang: *Appl. Surf. Sci.*, 2014, vol. 292, pp. 658–64.
33. S.C. Troughton, A. Nominé, J. Dean, and T.W. Clyne: *Appl. Surf. Sci.*, 2016, vol. 389, pp. 260–69.
34. S.C. Troughton, A. Nominé, A.V. Nominé, G. Henrion, and T.W. Clyne: *Appl. Surf. Sci.*, 2015, vol. 359, pp. 405–11.
35. A. Nominé, S.C. Troughton, A.V. Nominé, G. Henrion, and T.W. Clyne: *Surf. Coat. Technol.*, 2015, vol. 269, pp. 125–30.
36. G.H. Lv, H. Chen, W.C. Gu, L. Li, E.W. Niu, and X.H. Zhang: *J. Mater. Process. Technol.*, 2008, vol. 208, pp. 9–13.
37. W. Gebarowski and S. Pietrzyk: *Arch. Metall. Mater.*, 2013, vol. 58, p. 4.
38. X. Hussein, R.O. Northwood, and D.O. Nie: *J. Vac. Sci. Technol. A*, 2010, vol. 28, pp. 766–73.
39. H. Li, S. Lu, X. Wu, and W. Qin: *Surf. Coat. Technol.*, 2015, vol. 269, pp. 220–27.
40. V. Dehnavi, X.Y. Liu, B.L. Luan, D.W. Shoesmith, and S. Rohani: *Surf. Coat. Technol.*, 2014, vol. 251, pp. 106–14.
41. M. Aliofkhazraei and A.S. Rouhaghdam: *Appl. Surf. Sci.*, 2012, vol. 258, pp. 2093–97.
42. E. McCafferty: *Introduction to Corrosion Science*, Springer, New York, 2013, pp. 135–51.
43. E. McCafferty: *Corros. Sci.*, 2005, vol. 47, pp. 3202–15.
44. A. Lasia: *Mod. Asp. Electrochem.*, 1999, vol. 32, pp. 143–248.
45. M.E. Orazem: *Electrochemical Impedance Spectroscopy*, Wiley, New Jersey, 2015, pp. 73–96.
46. M. Shokouhfar, C. Dehghanian, M. Montazeri, and A. Baradaran: *Appl. Surf. Sci.*, 2012, vol. 258, pp. 2416–23.
47. L. Hamadou, L. Aïnouche, A. Kadri, S.A.A. Yahia, and N. Benbrahim: *Electrochim. Acta.*, 2013, vol. 113, pp. 99–108.
48. R.O. Hussein, X. Nie, and D.O. Northwood: *Electrochim. Acta.*, 2013, vol. 112, pp. 111–19.
49. B. Hirschorn, M.E. Orazem, B. Tribollet, V. Vivier, I. Frateur, and M. Musiani: *Electrochim. Acta.*, 2010, vol. 55, pp. 6218–27.